ACADEMIC PRESS

Journal of Solid State Chemistry 169 (2002) 53–59

JOURNAL OF SOLID STATE CHEMISTRY

www.academicpress.com

Synthesis and structural characterisation of $Sr_3Al_{10}SiO_{20}$ by XRD and solid-state NMR

M. Capron, F. Fayon, J. Coutures, D. Massiot, and A. Douy*

Centre de Recherche sur les Matériaux à Haute Température-CNRS, 1D Ave de la Recherche Scientifique, 45071 Orléans Cedex 2, France

Received 11 March 2002; received in revised form 30 June 2002; accepted 20 August 2002

Abstract

The strontium aluminosilicate $Sr_3Al_{10}SiO_{20}$ has been synthesised by a spray-drying process and characterised by powder X-ray diffraction. It crystallises in the monoclinic $I2/m$ space group with the cell parameters $a = 14.394(2)$ Å, $b = 11.189(2)$ Å, $c = 4.904(1)$ Å, $\beta = 90.793(1)^\circ$, $Z = 2$. Its structure is built of double AlO_6 octahedra chains interconnected by AlO_4 and SiO_4 tetrahedra forming a three-dimensional channel-like network where the strontium cations are located. The distribution of aluminium and silicon cations in the different tetrahedral and octahedral sites of the structure was probed using ^{29}Si, ^{27}Al MAS and 3Q-MAS NMR.

Keywords: Strontium aluminosilicate; Solid-state NMR; Spray-drying; Aqueous synthesis; X-ray diffraction; Rietveld refinement

1. Introduction

Strontium aluminates have been studied and applied extensively as phosphors when activated by Eu^{2+} cations, owing to their excellent properties such as high quantum efficiency, long persistence phosphorescence and good stability [1]. Due to unique properties such as high strength, low density, chemical stability, low thermal expansion and low dielectric constant, rare-earth aluminosilicate glass-ceramics have been used for various purposes including high-temperature structural applications and electronic packaging [2]. However, despite numerous similarities with their calcium counterparts, strontium aluminates and aluminosilicates have received less interest. Their phase diagrams and the overall chemical properties are not yet completely known. In the Al_2O_3–SiO_2–SrO phase diagram [3] three ternary compounds are reported. Two of them, $SrAl_2Si_2O_8$ and $Sr_2Al_2SiO_7$, are the strontium analogues of anorthite $CaAl_2Si_2O_8$ and gehlenite $Ca_2Al_2SiO_7$ and have been extensively studied, whereas the third compound, with the reported formula $Sr_6Al_{18}Si_2O_{37}$, is much less known. Its X-ray diagram has been identified [4] but its structure has not been determined. However, from our study of the Al_2O_3–SiO_2–SrO phase diagram, the reported X-ray diagram of "$Sr_6Al_{18}Si_2O_{37}$" is exactly reproduced only for the composition $3SrO.5Al_2O_3.SiO_2$. This diagram being strongly analogous with those of $Pb_3Al_{10}SiO_{20}$ and $Pb_3Al_{10}GeO_{20}$ [5], we conclude that the actual formula is $Sr_3Al_{10}SiO_{20}$. In the present work, we describe the synthesis of $Sr_3Al_{10}SiO_{20}$ by a spray-drying process and its structural characterisation by X-ray diffraction (XRD), ^{29}Si and ^{27}Al high-resolution solid-state NMR spectroscopy.

2. Experimental

2.1. Synthesis

Amorphous precursors of composition $3SrO$–$5Al_2O_3$–SiO_2 were synthesised using a spray-drying process. Aluminium nitrate nonahydrate $Al(NO_3)_3 \cdot 9H_2O$ and strontium nitrate $Sr(NO_3)_2$ (Aldrich) were the chemical sources for aluminium and strontium. Due to some uncertainty about their hydration, especially for the amount of water of crystallisation of the aluminium salt, their exact cation contents were

*Corresponding author. Fax: +33-38-638103.
E-mail address: douy@admin.cnrs-orleans.fr (A. Douy).

0022-4596/02/$ - see front matter © 2002 Elsevier Science (USA). All rights reserved.
PII: S0022-4596(02)00016-6

carefully determined by thermogravimetry. Tetraethoxysilane (TEOS) $Si(OC_2H_5)_4$ (Aldrich) was added to an aqueous solution of the two nitrates in the stoichiometric ratio and the mixture was magnetically stirred for 1 h, giving, after hydrolysis of TEOS, a clear precursor solution of aluminium and strontium nitrates and silicic acid. To reduce the ^{29}Si NMR relaxation time, gadolinium nitrate was added to the solution in order to have a 0.04 wt% concentration of Gd_2O_3 in the final oxide. The solution was spray-dried with compressed air in a laboratory apparatus (Büchi 190 mini spray-drier equipped with a 0.5 mm nozzle) operating at 200°C. The obtained powder was first calcined in a ventilated furnace at 800°C for 1 h to eliminate the nitrate and hydroxyl residues and then heated at different temperatures to study the different steps of the crystallisation process of $Sr_3Al_{10}SiO_{20}$.

2.2. Characterisation

The XRD powder patterns were collected at room temperature on a Philips PW1729 diffractometer (Cu$K\alpha$ radiation) in flat plate $\theta/2\theta$ geometry. Data were recorded in the 2θ range of 5–90° by steps of 0.02° with a scan time of 10 s per step.

The differential scanning calorimetry (DSC) analysis (Setaram, Caluire, France) was carried out at 5°C/min heating rate in air atmosphere.

The ^{29}Si magic angle spinning (MAS) NMR experiments were performed at room temperature on a Bruker DSX300 spectrometer (7.0 T) operating at a Larmor frequency of 59.6 MHz for ^{29}Si with a 7 mm MAS probehead. The ^{29}Si MAS NMR spectra were obtained at 4 kHz spinning rate using a single pulse excitation ($\pi/10$) with a recycle delay of 15 s to prevent saturation. The ^{27}Al solid-state NMR experiments were carried out on DSX Bruker spectrometers with magnetic field strengths of 7.0, 9.4 and 14.1 T, operating at ^{27}Al Larmor frequencies of 78.2, 104.3 and 156.4 MHz respectively and using 4 mm MAS and 2.5 mm high-speed MAS probeheads. The ^{27}Al MAS NMR spectra were recorded at spinning rates ranging from 13 to 35 kHz using a single pulse excitation sequence with small pulse angle ($\pi/12$) to ensure a quantitative excitation of the central transitions [6] and recycle delay of 4 s. The ^{27}Al triple-quantum MAS (3Q-MAS) spectra [7] were recorded at 9.4 T using the shifted-echo pulse sequence [8] while spinning at 15 kHz. To avoid sidebands in the ω_1 dimension and improve the sensitivity, the t_1 time increment was synchronised with the rotor period [9]. The two-dimensional pure absorption phase spectrum was obtained using the hypercomplex method [10]. The ^{29}Si and ^{27}Al chemical shifts were referenced relative to $Si(CH_3)_4$ and 1 M $Al(NO_3)_3$ aqueous solution, respectively.

3. Results and discussion

3.1. Synthesis and structure determination

The precursor powder was synthesised by a non-conventional process, since TEOS, the silicon alkoxide, was directly hydrolysed into an aqueous solution of strontium and aluminium nitrates. TEOS being not miscible with aqueous solutions, its hydrolysis is catalysed under stirring by the acidity of the nitrates solution [11]. The mixture turns into a clear solution of strontium and aluminium nitrates and silicic acid. In dilute solution and acidic pH, the condensation of silicic acid into silica is very low [11]. Spray-drying such aqueous solutions of metal nitrates and silicic acid, followed by heat treatment to decompose the nitrates, is a very simple process that has proved to be efficient in the synthesis of very chemically homogeneous amorphous precursors of silicates, like mullite [12,13] or magnesium silicates [14], and aluminosilicates, like cordierite [15]. In the present case, as usually for this process, TEOS being hydrolysed, no metallic element can be specifically lost by spray-drying, and thus the final composition of the mixed oxide is simply determined by a careful control of the stoichiometry of these elements in the starting solution. This is confirmed by a chemical analysis of the final product calcined at 1450°C (Table 1). The analysed weight ratio Al/Sr, 1.049, is closer to the theoretical 1.033 of the formula $Sr_3Al_{10}SiO_{20}$ than to 0.92 corresponding to the formula $Sr_6Al_{18}Si_2O_{37}$ originally reported [3,4].

The DSC trace (5°C/min) of the amorphous precursor of composition $3SrO–5Al_2O_3–SiO_2$ is shown in Fig. 1. This curve exhibits a first intense sharp

Table 1
Chemical analysis of $Sr_3Al_{10}SiO_{20}$

Weight %	Sr	Al	Si
Calculated	29.84	30.63	3.19
Analysed	28.6±0.6	30.0±0.6	3.0±0.1

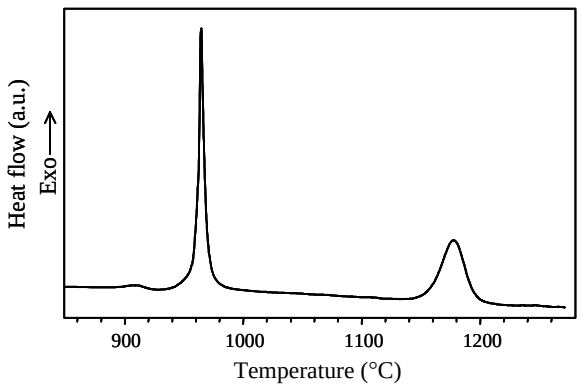

Fig. 1. DSC curve of the spray-dried powder; heating rate: 5°C/min.

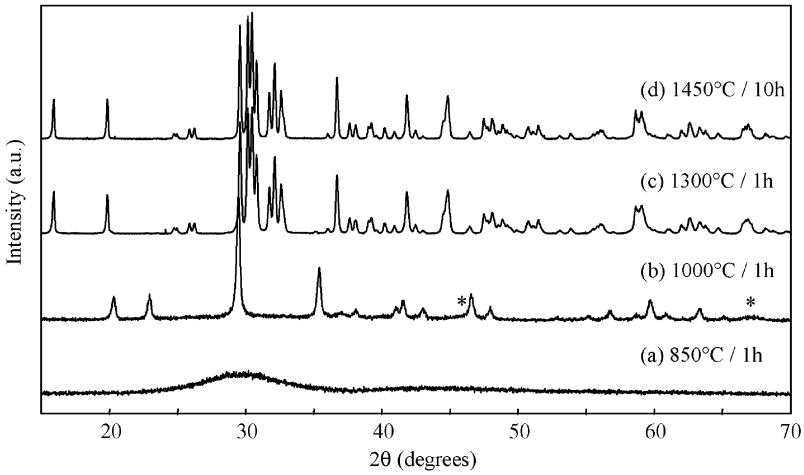

Fig. 2. X-ray diffraction powder patterns of the $3SrO–5Al_2O_3–SiO_2$ spray-dried sample annealed at the indicated temperatures. The broad and weak peaks of γ-Al_2O_3 solid solution are indicated by the asterisks.

exothermic peak located at 960°C with an enthalpy of 147 J/g and a second exothermic peak that occurs at 1180°C with an enthalpy of 109 J/g.

The XRD powder pattern of the sample heated at 1000°C for 1 h and cooled to room temperature is depicted in Fig. 2. It evidences the high-temperature metastable hexagonal phase of $SrAl_2O_4$($a = 5.10$ Å, $c = 8.45$ Å, JCPDS file 31-1336) [16] and also reveals the presence of γ-alumina solid solution, as indicated by the very broad and weak peaks at 46° and 67° 2θ characteristic of this high defect spinel phase. The $SrAl_2O_4$ hexagonal phase is not expected at room temperature, but current work in our laboratory has shown that it may be easily stabilised by incorporating silicon, calcium or excess aluminium cations. On the other hand, a high level of these cations (Si, Ca, Sr) can also be inserted in the γ-alumina structure using the same spray-drying process [13,17,18]. After the first crystallisation peak, the sample is a mixture of hexagonal $SrAl_2O_4$ and γ-alumina solid solutions, both phases probably inserting silicon atoms in their structures.

The XRD pattern of the sample heated at 1300°C for 1 h, shown in Fig. 2, is similar to that previously reported for "$Sr_6Al_{18}Si_2O_{37}$" [4] (JCPDS file 10-0025). However, according to the initial stoichiometry, confirmed by chemical analysis, and to the strong analogy between the experimental XRD diagram and those reported for $Pb_3Al_{10}SiO_{20}$ and $Pb_3Al_{10}GeO_{20}$ [5], the actual formula becomes $Sr_3Al_{10}SiO_{20}$. The second crystallisation peak occurring at 1180°C is therefore associated to the formation of $Sr_3Al_{10}SiO_{20}$. It should be mentioned that this XRD pattern also evidences a residual trace of the $SrAl_2O_4$ hexagonal phase. After annealing at 1450°C for 10 h, this secondary phase has completely disappeared. This sample was used for the structural characterisation.

$Sr_3Al_{10}SiO_{20}$ is an equilibrium phase in the $SrO–Al_2O_3–SiO_2$ system. The XRD diagram is unchanged after annealing at 1600°C. This compound may be synthesised by the solid-state reaction between SiO_2, Al_2O_3 and $SrCO_3$; heating a few hours at 1600°C yields single phase $Sr_3Al_{10}SiO_{20}$.

Assuming a monoclinic cell and the $I2/m$ space group, like for $Pb_3Al_{10}SiO_{20}$ [5], the structure of $Sr_3Al_{10}SiO_{20}$ was refined from the Rietveld profile analysis [19] of the XRD powder pattern using the FULLPROF program [20]. The Sr atoms were first located using the atomic coordinates of Pb in $Pb_3Al_{10}SiO_{20}$ at the initial step, and then the remaining atoms were deduced from subsequent Fourier difference calculations. Since the scattering factors of Al and Si are very similar, the Si atoms were assumed to be randomly distributed at the positions of the Al atoms. Fig. 3 shows the Rietveld refinement of $Sr_3Al_{10}SiO_{20}$. The principal crystallochemical data and conditions for intensity collection are summarised in Table 2. The final atomic coordinates and equivalent isotropic thermal parameters are given in Table 3.

The three-dimensional structure of $Sr_3Al_{10}SiO_{20}$ is built of AlO_6 octahedra and TO_4 tetrahedra occupied both by aluminium and silicon atoms. By edge sharing, the AlO_6 units form double octahedra chains parallel to the c-axis. The TO_4 tetrahedra are linked by corner forming layers in the (b, c) plane connected by the double octahedra chains. The Sr^{2+} cations are located in the tunnels running parallel to the c-axis of the structure (Fig. 4). The inter-atomic distances are very similar to those encountered in the $Pb_3Al_{10}SiO_{20}$ isostructural compound [5]. The Sr–O distances range from 2.35 to 2.82 Å and are slightly shorter than those of Pb–O (2.36–2.86 Å) as expected from the ionic radii of Sr^{2+} and Pb^{2+} [21]. For the two crystallographically non-equivalent AlO_6 sites (Al(1), Al(2)), the Al–O distances

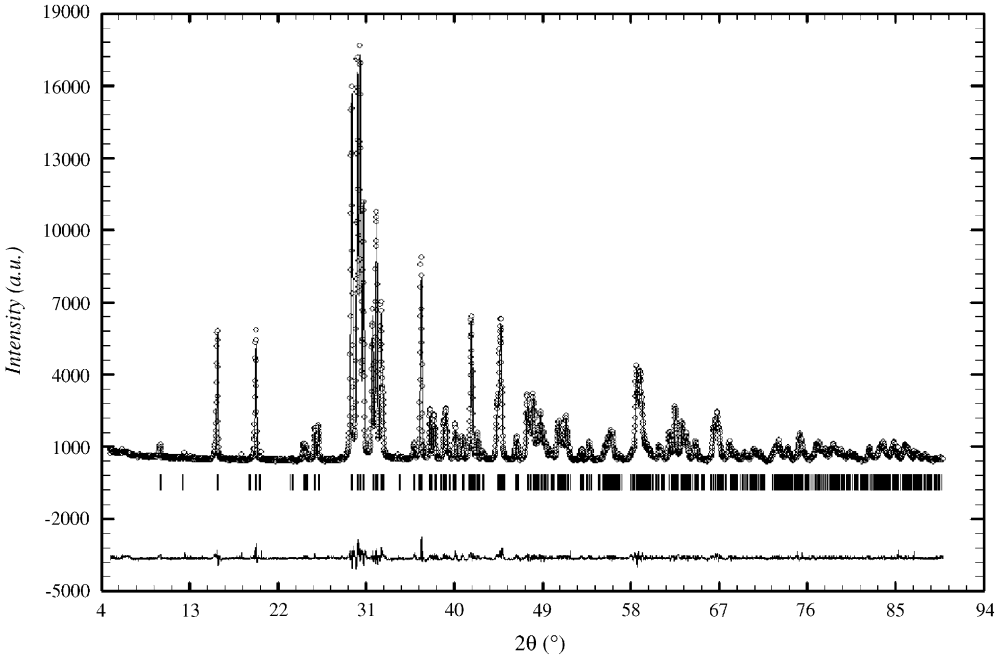

Fig. 3. Observed and calculated X-ray diffraction profiles (upper) together with their difference plots (lower) of the Rietveld refinement of $Sr_3Al_{10}SiO_{20}$; tick marks represent the positions of the Bragg reflections.

Table 2
Crystallographic data for $Sr_3Al_{10}SiO_{20}$

Chemical formula	$Sr_3Al_{10}SiO_{20}$
Formula weight (g/mol[1])	880.75
Symmetry	Monoclinic
Space group	$I2/m$
a(Å)	14.394(2)
b(Å)	11.189(2)
c(Å)	4.904(1)
β(deg)	90.793(1)
V (Å^3)	789.74(2)
Z	2
$\rho_{calc.}$ (g/cm^3)	3.69
Diffractometer	Philips PW 1729
2θ range (Cu$K\alpha$)	5–90°
Number of reflections	1224
Independent reflections	340
Average FWHM (deg)	0.1957
Number of refined parameters	65
[a]R_p (%)	3.63
[b]R_{wp} (%)	4.95
R_{exp} (%)	3.09
Chi^2	2.58

[a] $R_p = \sum[|F_o - F_c|]/\sum|F_o|$.
[b] $R_{wp} = [\sum w(|F_o| - |F_c|)^2/\sum w|F_o|^2]^{1/2}$.

vary from 1.86 to 1.94 Å, while for the two crystallographically non-equivalent tetrahedral sites (T_1, T_2), the M–O distances (M = Si or Al) range from 1.71 to 1.76 Å. To go further in the description of the ordering of Si and Al atoms in the two distinct tetrahedral sites of the structure, ^{29}Si and ^{27}Al solid-state NMR experiments have been carried out.

3.2. Solid-state NMR characterisation

As shown in Fig. 5, the ^{29}Si MAS NMR spectrum of crystalline $Sr_3Al_{10}SiO_{20}$ exhibits a narrow resonance located at about −80.5 ppm characteristic of fourfold coordinated Si atoms, with an FWHM of 2.5 ppm typical of crystalline phases. The lineshape of the resonance is slightly asymmetric showing a shoulder at the high-field side. A good fit of the experimental spectrum can only be obtained using two contributions with isotropic chemical shifts of about −80 and −81 ppm. In the structure, the two tetrahedral sites T_1 and T_2 can be distinguished according to their connectivities. The T_1 site is linked to three tetrahedral T_2 sites through bridging bonds (Q_3 unit), the remaining oxygen atom of the tetrahedron being shared with two AlO_6 octahedra, while the T_2 site is linked to four tetrahedral sites (Q_4 unit). According to the ^{29}Si chemical shift ranges in aluminosilicates [22,23], the two components at −80 and −81 ppm can be attributed to the Q_3(3Al) and Q_4(4Al) species corresponding to the T_1 and T_2 sites of the structure, respectively. However, a quantitative determination of their relative populations remains ambiguous due to the lack of resolution in the ^{29}Si experimental spectrum. It should be mentioned that the presence of Si–O–Si linkages yielding significantly lower ^{29}Si chemical shift values is not observed in the

Table 3
Atomic coordinates and isotropic displacement parameters for $Sr_3Al_{10}SiO_{20}$

Atoms	Site	x	y	z	B_{eq} (Å^2)
Sr(1)	2*a*	0	0	0	3.45(5)
Sr(2)	4*i*	0.2831(1)	0	0.0218(3)	3.18(2)
Al(1)	2*b*	0	0.5	0	3.27(9)
Al(2)	4*h*	0.5	0.1288(3)	0	3.13(1)
T_1 (Al, Si)	8*j*	0.1366(3)	0.2872(2)	−0.0277(7)	2.63(9)
T_2 (Al, Si)	8*j*	0.3553(2)	0.3630(2)	0.0096(7)	2.70(8)
O(1)	4*i*	0.4339(6)	0	−0.1751(1)	2.71(1)
O(2)	4*i*	0.9007(5)	0	0.4196(1)	2.82(1)
O(3)	8*j*	0.2404(4)	0.3584(4)	−0.0827(1)	2.13(7)
O(4)	8*j*	0.4162(4)	0.2482(4)	−0.1559(9)	2.14(7)
O(5)	8*j*	0.8608(4)	0.1492(4)	−0.1343(1)	2.53(7)
O(6)	8*j*	1.0734(4)	0.3803(4)	0.1845(1)	2.10(8)

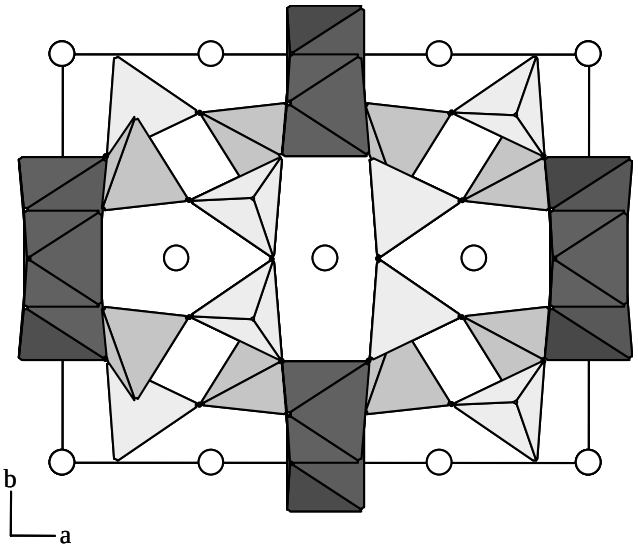

Fig. 4. Projection of the $Sr_3Al_{10}SiO_{20}$ structure along (0 0 1). The Sr atoms are drawn as hollow circles, the T_1 and T_2 tetrahedral sites in medium grey and light grey, respectively, and the AlO_6 octahedra in dark grey.

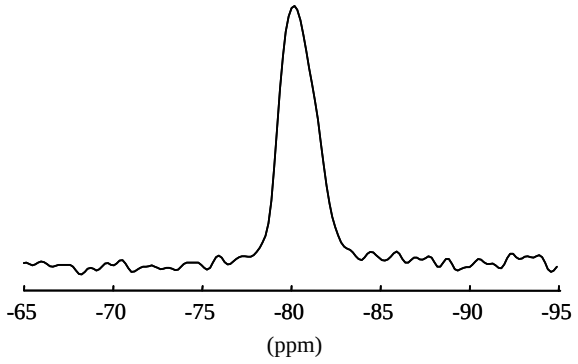

Fig. 5. ^{29}Si MAS NMR spectrum of $Sr_3Al_{10}SiO_{20}$($B_0 = 7.0$ T).

^{29}Si MAS spectrum, but a small amount of these linkages is not completely excluded due to the weak NMR sensitivity of ^{29}Si and the low silicon content in the sample.

The ^{27}Al MAS NMR spectra of $Sr_3Al_{10}SiO_{20}$ obtained at three different applied magnetic fields are shown in Fig. 6. These spectra clearly indicate the presence of several overlapping resonances in the frequency ranges characteristic of tetrahedral AlO_4 sites and octahedral AlO_6 sites. As expected for ^{27}Al, the variation in lineshape with the applied magnetic field suggests that the broadening of the lines is due to the second-order quadrupolar interaction. To obtain a ^{27}Al NMR spectrum with improved resolution, we have used the two-dimensional (2D) triple-quantum MAS (3Q-MAS) method [7] that allows to average out the second-order quadrupolar interaction. As shown in Fig. 7, two intense AlO_4 and one intense AlO_6 resonances are clearly resolved in the isotropic ω_1 dimension of the ^{27}Al 3Q-MAS spectrum recorded at 9.4 T. This spectrum also evidences an additional AlO_6 resonance with a lower intensity due to its larger quadrupolar coupling constant (C_Q) and the limited radio-frequency field strength used for the excitation of the triple quantum coherences. It should be noted that these lines show broadened asymmetric lineshape characteristic of a distribution of the quadrupolar interaction that reflects the structural disorder due to the Al/Si substitution in the tetrahedral sites. The ^{27}Al isotropic chemical shifts and quadrupolar parameters (including distributions) for the four resonances were determined from the simulation of the experimental 3Q-MAS spectrum [24] and are reported in Table 4. Using these parameters, good fits of the quantitative MAS spectra at the three applied fields were obtained (Fig. 6). This confirms the interpretation of the 3Q-MAS spectrum and allows a reliable quantitative interpretation to be derived. The integrated intensities of the two AlO_6 resonances corresponding to the two non-equivalent octahedral sites of the structure are approximately in the ratio 2:1 in good agreement with the site multiplicities. The most intense contribution ($\delta_{ISO} = 12$ ppm, $C_Q = 8.13$ MHz) is assigned to the Al(2) site and the remaining one ($\delta_{ISO} = 7.2$ ppm, $C_Q = 3.73$ MHz) to the Al(1) site of

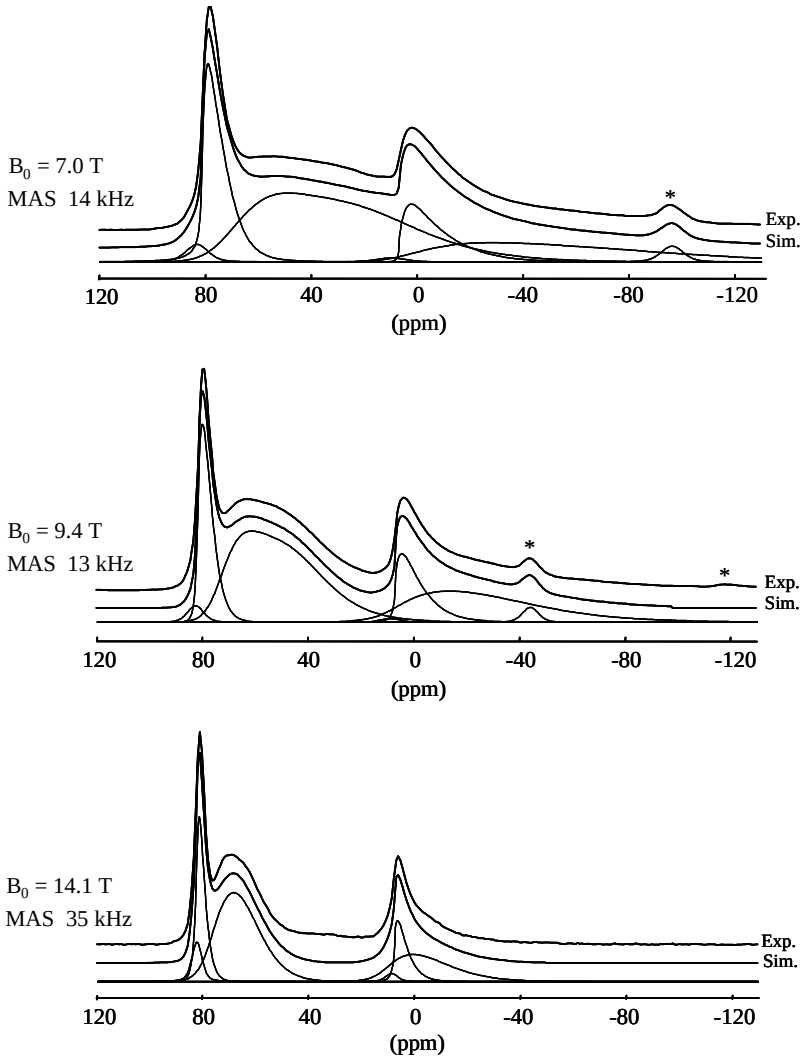

Fig. 6. Experimental ^{27}A1 MAS NMR spectra of $Sr_3Al_{10}SiO_{20}$ obtained at 7.0, 9.4 and 14.1 T and their simulations according to the parameters reported in Table 4. The asterisks mark spinning sidebands.

Table 4
^{27}Al isotropic chemical shifts, quadrupolar parameters and relative intensities obtained from the simulation of the ^{27}Al 3Q-MAS and MAS spectra of $Sr_3Al_{10}SiO_{20}$

Site	δ_{ISO} (ppm)	C_Q (MHz)	η_Q	ΔC_Q (MHz)	I (%)
Al(1)	7.2	3.73	0	1.13	10
Al(2)	12.0	8.13	0.3	1.33	20
T_2(4Al)	82.0	2.61	0	0.60	20
$T_1 + T_2$(nAl, mSi)	78.0	6.86	0.3	0.80	50

the structure. The proportion of AlO_4 and AlO_6 units in the structure determined from the quantitative ^{27}Al spectra is close to that expected from the crystallographic data, although the relative intensities of the two AlO_4 resonances differ significantly from the multiplicity of the T_1 and T_2 sites. This difference is not only explained by the presence of silicon in the tetrahedral sites but also reflects the sensitivity of the quadrupolar interaction to the symmetry of the ^{27}Al environment. In this case, the contribution with weaker C_Q value ($\delta_{ISO} = 82$ ppm, $C_Q = 2.61$ MHz) could be assigned to the more symmetric ^{27}Al environment of the structure that corresponds to T_2 sites with four adjacent tetrahedra occupied by aluminium atoms (T_2(4Al)), while the remaining resonance ($\delta_{ISO} =$ 78 ppm, $C_Q = 6.86$ MHz) could correspond to both T_1 sites and the remaining T_2 sites linked to SiO_4 tetrahedra ($T_2(n\text{Al}, m\text{Si})$). A more accurate discussion of the Al/Si ordering in the tetrahedral sites of the $Sr_3Al_{10}SiO_{20}$ structure would require a more detailed characterisation of the various ^{27}Al and ^{29}Si spatial relations that will be obtained from ^{29}Si/^{27}Al double resonance NMR experiments, currently under development.

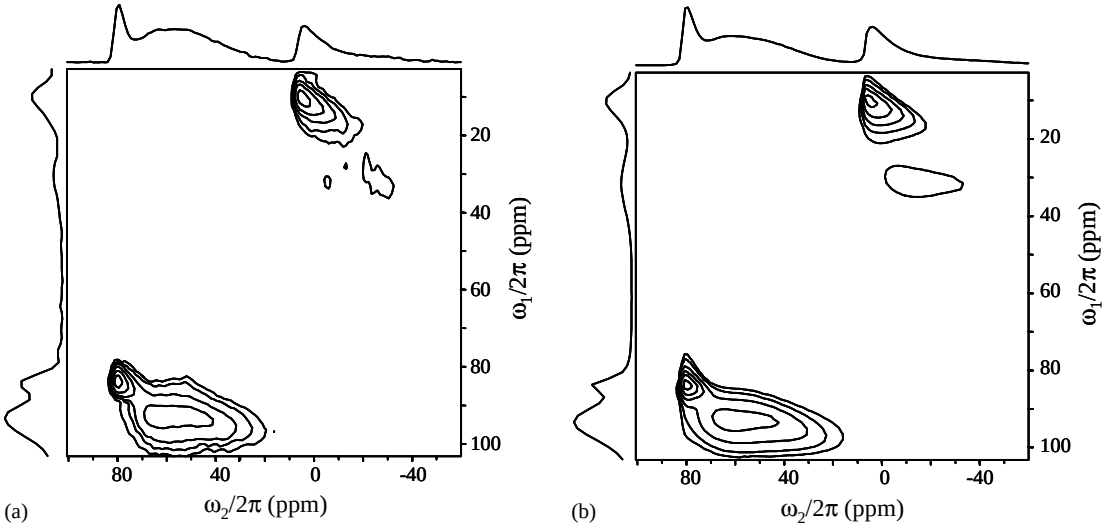

Fig. 7. Experimental (a) and simulated (b) ^{27}Al 3Q-MAS NMR spectra of $Sr_3Al_{10}SiO_{20}$ ($B_0 = 9.4$ T). The contour levels were set to 3.0%, 5.7%, 10.8%, 20.5%, 39.1% and 74.2% of the maximal peak intensity. The projections on the ω_1 (vertical) and ω_2 (horizontal) dimensions display isotropic and MAS spectra respectively.

Acknowledgments

We acknowledge financial support by CNRS, Région Centre and European Community contracts HPRI-CT-1999-00042 and HPMT-CT-2000-00169. Prof. G. Bodenhausen is thanked for providing access to the 600 MHz spectrometer at the ENS-Paris.

References

[1] B. Smets, J. Rutten, G. Hoeks, J. Verlijsdonk, J. Electrochem. Soc. 136 (1989) 2119.
[2] G.H. Beall, D.A. Duke, in: D.R. Uhlmann, N.J. Kreidl (Eds.), Glass Science and Technology, Vol. 1, Glass-Ceramic Technology, Academic Press, New York, 1983, p. 403.
[3] P.S. Dear, Bull. Virginia Polytechn. Inst. 50 (1957) 8.
[4] P.S. Dear, Bull. Virginia Polytechn. Inst. 50 (1957) 14.
[5] K. Vinek, H. Völlenkle, H. Nowotny, Monatsch. Chem. 101 (1970) 275.
[6] A. Samoson, E. Lippmaa, Phys. Rev. B 28 (1983) 6567.
[7] L. Frydman, J.S. Harwood, J. Am. Chem. Soc. 117 (1995) 5367.
[8] D. Massiot, B. Touzo, D. Trumeau, J.P. Coutures, J. Virlet, P. Florian, P.J. Grandinetti, Solid State NMR 6 (1996) 73.
[9] D. Massiot, J. Magn. Reson. A 122 (1996) 240.
[10] R.R. Ernst, G. Bodenhausen, A. Wokaun, Principles of Nuclear Magnetic Resonance in One and Two Dimensions, Clarendon Press, Oxford, 1987.
[11] R.K. Iler, The Chemistry of Silica, Wiley, New York, 1979.
[12] I. Jaymes, A. Douy, J. Am. Ceram. Soc. 75 (1992) 3154.
[13] I. Jaymes, A. Douy, M. Gervais, J.P. Coutures, J. Sol–Gel Sci. Technol. 8 (1997) 415.
[14] A. Douy, J. Sol–Gel Sci. Technol. 24 (2002) 221.
[15] A. Douy, J. Non-Cryst. Solids 147&148 (1992) 554.
[16] S. Ito, S. Banno, K. Suzuki, M. Inagaki, Z. Phys. Chem. 105 (1977) 173.
[17] A. Douy, in: D. Bortzmeier, M. Boussuge, Th. Chartier, G. Fantozzi, G. Lozes, A. Rousset (Eds.), Key Engineering Materials, Vol. 132–136, Euroceramics V, Part 1, Trans Tech Publications, Zurich, 1997, p. 101.
[18] A. Douy, M. Gervais, J. Am. Ceram. Soc. 83 (2000) 70.
[19] M.H. Rietveld, J. Appl. Crystallogr. 1969 (65).
[20] J. Rodriguez-Carvajal, FULLPROF version 3.5, Laboratoire Léon Brillouin, Saclay, France, October 1998.
[21] R.D. Shannon, C.T. Prewitt, Acta Crystallogr. B 25 (1969) 925.
[22] G. Engelhardt, D. Michel, High-resolution Solid-state NMR of Silicates and Zeolites, Wiley, New York, 1987.
[23] E. Lippmaa, A. Samoson, M. Mägi, J. Am. Chem. Soc. 108 (1986) 1730.
[24] D. Massiot, F. Fayon, M. Capron, I. King, S. Le Calvé, B. Alonso, J.O. Durand, B. Bujoli, Z. Gan, G. Hoatson, Magn. Reson. Chem. 40 (2002) 70.